Journal of Structural Geology 34 (2012) 77–90

Contents lists available at SciVerse ScienceDirect

Journal of Structural Geology

journal homepage: www.elsevier.com/locate/jsg

Origin and behavior of clay minerals in the Bogd fault gouge, Mongolia

M.D. Buatier [a,*], A. Chauvet [b], W. Kanitpanyacharoen [c], H.R. Wenk [c], J.F. Ritz [b], M. Jolivet [d]

[a] Chrono-Environnement, UMR 6249, Université de Franche Comté, 16 route de Gray Besançon 25030, France
[b] Géosciences Montpellier, UMR 5243, Université Montpellier 2, 34095 Montpellier Cedex 5, France
[c] Earth and Planetary Science, University of California, Berkeley, CA 94720, USA
[d] Géosciences Rennes, UMR 6118, Université Rennes 1, Campus de Beaulieu, 35042 Rennes Cedex, France

ARTICLE INFO

Article history:
Received 10 February 2011
Received in revised form
12 September 2011
Accepted 30 October 2011
Available online 9 November 2011

Keywords:
Clays
Gouge
Seismic fault
TEM
SEM
Texture

ABSTRACT

We analyzed twelve fault gouge samples from the Bogd fault in south-western Mongolia to understand the origin and behavior of clay minerals. The investigation relies on x-ray powder diffraction (XRD), scanning electron microscopy (SEM), transmission electron microscopy (TEM) and high energy synchrotron x-ray diffraction methods to investigate microstructure and preferred orientation. Smectite (montmorillonite), illite-smectite mixed layers, illite-mica and kaolinite are the major clay components, in addition to quartz and feldspars, which are present in all samples. The observations suggest that the protoliths and the fault rocks were highly altered by fluids. The fluid-rock interactions allow clay minerals to form, as well as alter feldspars to precipitate kaolinite and montmorillonite. Thus, newly formed clay minerals are heterogeneously distributed in the fault zone. The decrease of montmorillonite component of some of the highly deformed samples also suggests that dehydration processes during deformation were leading to illite precipitation. Based on synchrotron x-ray diffraction data, the degree of preferred orientation of constituent clay minerals is weak, with maxima for (001) ranging from 1.3 to 2.6 multiples of a random distribution (m.r.d). Co-existing quartz and feldspars have random orientation distributions. Microstructure and texture observations of the gouges from the foliated microscopic zone, alternating with micrometric isotropic clay-rich area, also indicate that the Bogd fault experienced brittle and ductile deformation episodes. The clay minerals may contribute to a slip weakening behavior of the fault.

1. Introduction

Fault gouge is located in a highly deformed zone resulting from localization of shear (Mair and Abe, 2008; Rutter et al., 1986). It is characterized by very fine-grained materials produced by cataclasis during tectonic movements. Clay is generally the dominant mineral group in the fault gouge but can be formed over a wide range of environmental conditions. Clay minerals also have high cation exchange capacity and large specific surface area, allowing adsorption of water molecules (Hofmann et al., 1933). The attraction between dipoles of water molecules and electrically charged clay surfaces can significantly decrease strength of fault gouge (Bird, 1984; Morrow et al., 2000). Expandable clays in the smectite-group, particularly the most common member such as montmorillonite, can take a great amount of interlayer water into the crystal structure (Bird, 1984). Moreover, the preferred orientation of constituent clays can play a crucial role on fault behaviors, for instance, controlling frictional and hydrological properties, and affecting permeability and slip rate of the faults (Haines et al., 2009; Rice, 1992; Vrolijk and van der Pluijm, 1999). These unique characteristics of clays have caught attention of geologists as they have important implications on the stability and strength of fault mechanics. Thus, a number of experimental studies of the microtextural evolution and mechanical properties of clay-bearing fault gouge have been carried out (Bird, 1984; Haines et al., 2009; Mizoguchi et al., 2009; Morrow et al., 2000; Rutter et al., 1986). However, the investigation of clay minerals in natural fault gouges is very challenging due to small grain size, poor crystallinity and various clay growth processes in the same location. For example, authigenic clays can be produced by fluid-rock interaction or direct precipitation from circulating fluids. Furthermore, synkinematic clay minerals are produced by deformation that commonly requires the presence of fluids (i.e. Dellisanti et al., 2008; Day-Stirrat et al., 2008).

The aim of this study is to investigate microstructure and preferred orientation of clays at various scales in order to have

* Corresponding author. Tel.: +33 (0) 3 81 66 65 61; fax: +33 (0) 3 81 66 65 58.
E-mail address: martine.buatier@univ-fcomte.fr (M.D. Buatier).

0191-8141/$ – see front matter © 2011 Elsevier Ltd. All rights reserved.
doi:10.1016/j.jsg.2011.10.006

a better understanding of their characteristics and formation processes in fault gouge. We used twelve gouge samples from the seismogenic Bogd fault in southern Mongolia (Florensov and Solonenko, 1965; Ritz et al., 1995; Kurushin et al., 1997). Samples were first investigated with x-ray power diffraction (XRD) for mineralogical composition and then analyzed with scanning electron microscopy (SEM) for microstructure. Two selected samples (BO25 from Bitut and BO20D from Noyon Uul) were examined with transmission electron microscopy (TEM) techniques for clay structures in fine detail. Synchrotron x-ray diffraction method, which has been shown to be able to successfully characterize composition and crystallographic preferred orientation (the term fabric or texture is used interchangeably) of natural and experimentally produced clay-rich samples (Kanitpanyacharoen et al., in press; Voltolini et al., 2009; Wenk et al., 2008a, 2010), was also employed on three gouge samples (BO20D, BO20E and BO24O). A Rietveld data analysis (Rietveld, 1969) was applied to extract quantitative texture information of constituent minerals from diffraction images. Our texture analysis of the Bogd fault is also compared with other fault systems such as the San Andreas (Janssen et al., 2010; Schleicher et al., 2009; Wenk et al., 2010) and the Punchbowl faults in California (Schulz and Evans, 1998), the Moab fault in Utah (Solum et al., 2005), the Nojima fault zone in Japan (Shimamoto et al., 2001), and the Alpine fault in New Zealand (Warr and Cox, 2001).

2. Geological setting and sample selection

We selected twelve samples from the Bogd fault system in southern Mongolia that experienced a magnitude 8.3 Gobi-Altay earthquake in 1957 (Florensov and Solonenko, 1965; Baljinnyam et al., 1993; Kurushin et al., 1997; Ritz et al., 1995). The Bogd fault belongs to the Gurvan Bogd fault system that formed the easternmost part of the Gobi-Altay mountain range (Fig. 1). The Bogd fault corresponds to a N100°E trending, 260 km long left-lateral strike-slip fault zone, bounding to the North the Ih Bogd and Baga Bogd massifs, two 50 km long, 20 km wide mountain ranges situated within restraining bends (Fig. 1). We studied the Bogd and paleo-Bogd faults located at the northern limit of the Ih Bogd massif. The Bogd and paleo-Bogd faults have a sinistral reverse kinematics as illustrated at the outcrop scale (Fig. 2). Both faults were re-activated during the late Cenozoic from inherited Paleozoic and Mesozoic structures (Florensov and Solonenko, 1965; Ritz et al., 2006; Jolivet et al., 2007; Vassallo et al., 2007a, 2007b).

Four gouge and two protolith samples were collected from the Bogd fault at the Noyan Uul location. In the following discussion, we refer the samples as BO17, BO20B, BO13C, BO19, BO20D and BO20E. The active Noyan Uul fault forms the base of a 40 m thick deformation zone characterized by multiple and alternating faults and cataclastic layers (Fig. 2A). The fault trends N100°E and steeply dips towards the south. The frontal part of the fault F_0

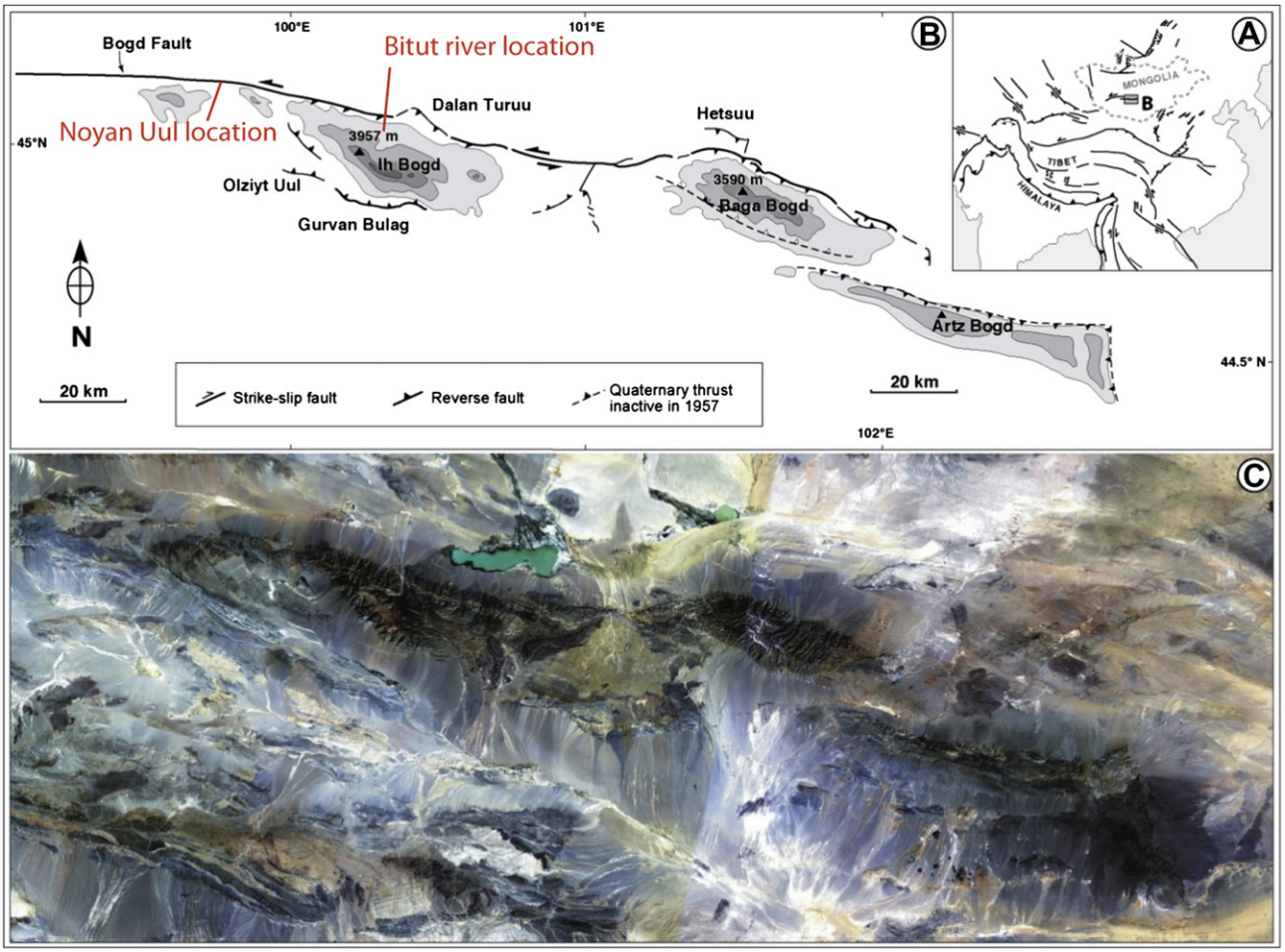

Fig. 1. Location of the studied faults in the Gobi-Altai massif (Mongolia) (A and B) and aerial photograph of the studied area (C) (modified after Ritz et al., 2006).

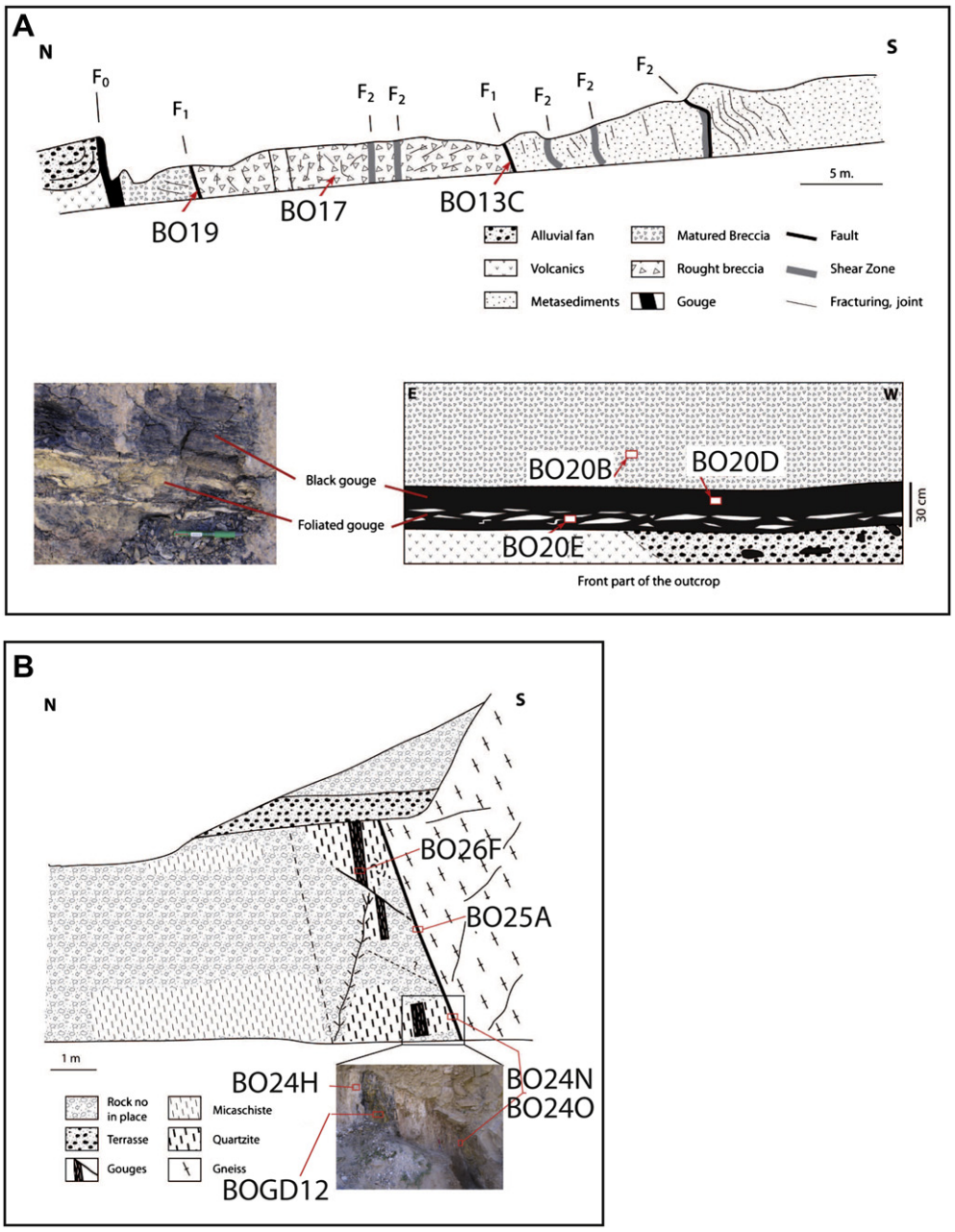

Fig. 2. A - Field description of the Bogd fault at Noyon Uul, location. The cross section represents the lithological succession observed along the Bogd fault. Faults numbers are related to their respective chronology. F_0 is the younger, F_2, the older. Other illustrations show a front view of the F_0 fault (sketch and photograph). Sample locations referred to the text are indicated. B - Outcrop description of the PaleoBogd fault at the Bitut location showing the gouge distribution within the different lithologies. Two gouge generations can be seen in the figure (see text). Sample locations are indicated.

(samples BO20D and BO20E) displays evidence of recent seismic activity with alluvial fan conglomerates that are part of the frontal peneplain domain. At this location, the fault is characterized by a 50 cm thick gouge divided into two distinct parts, (a) a 20 cm thick foliated gouge with sinistral shearing (BO20E) and (b) a 20 cm thin black homogeneous gouge (BO20D). These two parts can be clearly distinguished as shown in Fig. 2A. White lenses represent cataclastically-deformed relict host-rock. We also sample the host rocks situated above the black gouge level (sample BO20B).

Five additional fault gouge and one protolith samples were obtained from the paleo-Bogd fault at the Bitut river (Figs. 1 and 2B). The paleo-Bogd is roughly 15 m thick, complex and inactive fault zone. A 2 cm thick black gouge forms a thin boundary separating, gneiss in the southern part of the fault, and metasedimentary quartzite and mica-schist on northern section (Fig. 2B). A 30 cm thick black and white foliated gouge is also developed within a white quartzite unit. The shear zone contains at least two generations of gouge that are visible as displayed in Fig. 2B and numerous shear criteria indicates a reverse sinistral motion. The composition and microstructure of the fault is generally heterogeneous; thus three different types of samples were collected. Sample BOGD12 and BO26F are from the thick black and white gouge, samples BO24O, BO24N and BO25A are from the thin black gouge and sample BO24H is from the quartzite protolith (Fig. 2B).

3. Experimental methods

3.1. X-ray powder diffraction (XRD)

XRD analyses of bulk sediment samples were conducted at the Geological Institute of the University of Neuchatel with a Sintag 2000 diffractometer using Cu-Kα radiation and Germanium crystal Kevex detector. Diffraction patterns were obtained with 2θ range from >0 to 60° at a scan speed of 0.5°/min. The XRD was operating with an accelerating voltage of 45 kV and current of 40 mA, with 0.1°–1° opening slits. Samples were prepared by grinding roughly 800 mg of sediments into fine power and pressing at about 20 MPa in a powder holder covered with a blotting paper. More details about the procedure can be found in Kübler (1987). Relative abundances of minerals were estimated qualitatively based on the diffraction peak heights without interferences. In order to determine the nature of clay minerals, oriented preparations of the extracted. <2 μm and 2–16 μm fractions were collected on glass slides and sequentially air-dried, and ethylene-glycol treated before their XRD analyses. To improve the measurement of the positions of the diffraction peaks, XRD reflections around 7–9°2 θ were decomposed into elementary Pearson curves using free Mac Diff XRD software (http://www.geologie.uni-frankfurt.de/staff/Homepages/Petschick/MacDiff/MacDiffInfoE.html). The illite cristallinity (IC) was determined by the measurement of the mean full width at half maximum intensity of the 10 Å peak after decomposition.

3.2. Scanning electron microscopy (SEM)

Polished thin sections of all samples from the two locations were carbon coated and examined for petrographic analyses with a Jeol 5600 SEM equipped with a Fondis EDS detector. SEM micrographs were collected in both secondary electron and backscattered electron modes. The observations were done at the Centre Commun de Microscopie of Université de Franche Comté in Besançon. The SEM was operated with an accelerating voltage of 20 kV. The samples were also analyzed for mineralogical composition with the EDS Fondis detector.

3.3. Transmission electron microscope (TEM)

Samples were obtained from two black gouges at the Bitut (BO25A) and Noyan Uul (BO20D) locations for TEM analyses. Two types of TEM preparations were made. Both samples were impregnated in a Spurr resin, cut with a diamond knife on an ultramicrotome, and mounted on carbon coated Cu grids. More details of the microtome method can be found in Tessier (1984) and Elsass et al. (1998). The same samples were epoxy impregnated, thin sectioned, mounted on cupper grids and ion-milled with a Gatan Argon ionmill. TEM observations were made with a Jeol 2000FX system operating at 200 KV at the Center of Analysis (ARCEN) of the University of Bourgogne (Dijon).

3.4. Synchrotron x-ray texture measurement

Three fault gouge samples (BO20E, BO24O and BO20D) were embedded in a low-temperature hardening epoxy resin for 48 h. After being completely dry, each specimen was cut with a thin-bladed diamond saw into a slice approximately 2 cm in diameter and 1 mm thick for x-ray diffraction measurements. Kerosene was used as a cooling and polishing agent to prevent clay expansion. The experiments were conducted at beamline BESSRC 11-ID-C of the Advance Photon Source (APS) at Argonne National Laboratory. A monochromatic X-ray beam with a wavelength of 0.10779 Å and a diameter of 0.5 mm was used. Each sample was mounted to an aluminum rod perpendicular to the incident x-ray on a goniometer. The sample was translated over 2 cm parallel to the rod during x-ray exposure to obtain a representative sample volume. The sample was analyzed in transmission and diffraction patterns were collected for 60 s and recorded 2θ angle range from 0° to 4.6° with a Mar345 image plate, situated roughly 2 m away from the sample. The sample was also tilted around the rod axis from −45° to 45° in 15° intervals, thus recording 7 diffraction images to improve the pole figure coverage.

The diffraction images were then integrated from 0° to 360° azimuth over 10° sectors to produce 36 spectra. These spectra were calibrated with a CeO_2 standard to refine instrumental parameters for sample-detector distance, beam center and image plate tilt. Each spectrum represents distinctively oriented lattice planes and clearly shows peak intensity variation with azimuth. The diffraction data were analyzed for texture information with the Rietveld method (Rietveld, 1969) implemented in MAUD (Material Analysis Using Diffraction) software (Lutterrotti et al., 1997). The Rietveld refinement relies on a least-squares approach to minimize the difference between experimental diffraction data (Exp.) and a calculated diffraction model (Calc.). Our models refined several factors such as instrumental parameters, scattering background (polynomial functions), crystal structure, microstructure, weight fraction of each phase and its preferred orientation. The spectra are expressed as function of $Q = 2\pi/d$ rather than d (lattice spacing) to avoid compression of spectrum towards small d-spacings. A Q range of 0.22–3.56 $Å^{-1}$ (d-spacing: 1.70–31 Å, 2θ: 0.2–3.5°) was used for the refinement.

We used crystal structure parameters for triclinic kaolinite (Bish, 1993), monoclinic illite-mica (Gualtieri, 2000), monoclinic montmorillonite (Lutterotti et al., 2010), quartz and andesine from the database contained in MAUD. The diffraction peak shapes and widths were modeled by refining crystallite size and microstrain. Quartz and andesine were refined with an isotropic crystallite size model while the clay phases were refined with Popa rules to describe anisotropic crystallite shape (Popa, 1998). Stacking disorder of montmorillonite layers was also modeled by implementing 10 layers along the a-axis in MAUD (Lutterotti et al., 2010; Ufer et al., 2004). This is suitable for fitting peak asymmetries as a result of turbostatically stacking disorder.

Information about preferred orientation (texture) was extracted by the EWIMV algorithm (Matthies and Vinel, 1982), using 10° resolution for the determination of the Orientation Distribution Function (ODF), without imposing sample symmetry. The ODF, which defines the crystallite orientation relative to sample coordinates, was exported from MAUD and imported into the BEARTEX software (Wenk et al., 1998). First the ODF was smoothed with a 7.5° filter to minimize artifacts from the cell structure. Then the sample was rotated so that pole figures of phyllosilicates have the distinct (001) maximum near the center. The pole densities are expressed as multiples of random distribution (m.r.d.). In clay minerals the basal plane (001) is most significant, thus we show the (001) pole figures and in addition (100) pole figures to establish if there are constraints on the orientation of a-axes). The same scale is used for all phases.

4. Results

4.1. Mineralogical characterization

4.1.1. The protoliths

The two protolith samples (BO17 and BO20B) from Noyan Uul were collected from the cataclastic rocks located at the top of the fault gouge. Cataclasis strongly affected the outcrop, thus it is

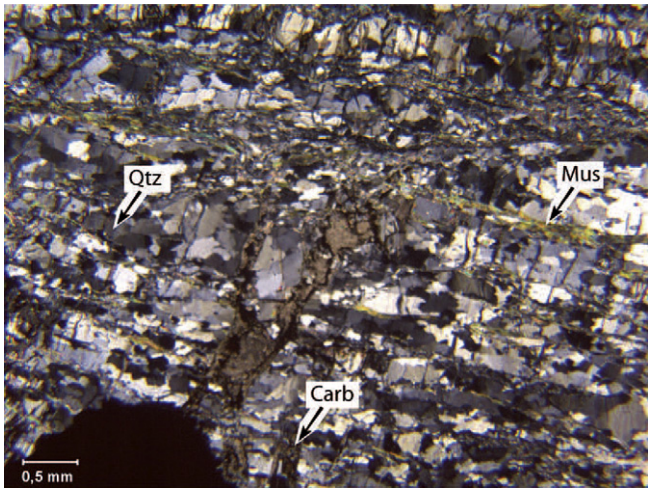

Fig. 3. Thin section of the quartzite unit at the Bitut location. Note the specific mineralogy with dominant quartz and mica grains affected by carbonate veins. Qtz = quartz, mus = muscovite, carb = ankerite.

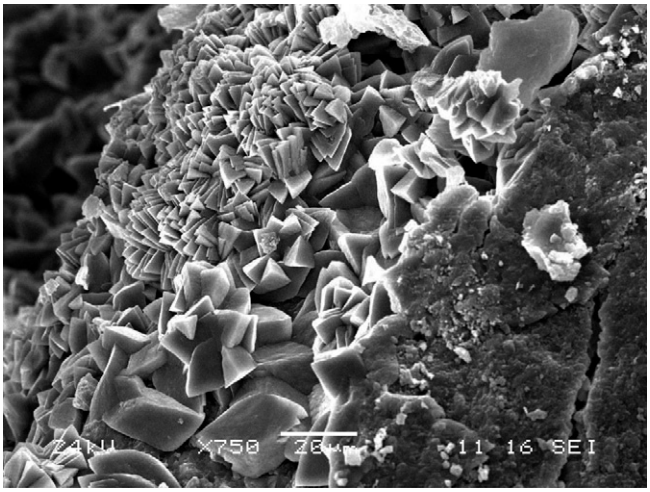

Fig. 4. Scanning electron microscopy (SEM) in secondary electron imaging mode of newly formed ankerite crystal in the protolith gneiss from Noyon Uul.

difficult to determine if the two samples come from the same lithological unit of Noyan Uul. In contrast, sample from the Bitut area does not exhibit any trace of cataclasis (Fig. 3). According to XRD analyses and optical microscopic observations, quartz, feldspars, ankerite and kaolinite are present in all samples but in different proportions (Table 1). Feldspars is a major phase in BO17, which can correspond to an altered gneiss, whereas quartz is dominant in BO20B. BO24H is a quartz schist from the Bitut outcrop and mostly composed of mica and quartz with minor feldspars (Fig. 3 and Table 1). XRD data and SEM images suggest that all protolith samples have secondary mineral phases. For example, kaolinite replaces feldspars and newly formed ankerite crystals are observed as aggregates of euhedral crystals filling secondary porosity (Fig. 4).

According to XRD analyses on sediments with a grain size <2 μm, kaolinite is as a major clay phase, while illite or/and smectite (montmorillonite) are found to be relatively less abundant (Table 1). The diffraction pattern of BO17 displays a strong reflection at 12.8 Å which later expands to 17 Å upon glycolation, suggesting the presence of smectite (montmorillonite). A diffraction peak at 10 Å displays an asymmetric shape at low 2θ angle implying the presence of smectite and/or illite-smectite mixed layers in BO20B and BO24H samples (Table 1).

4.1.2. Fault gouges

According XRD data on sample BO20D, BO20E, BO13C and BO19, the black fault gouges at Noyan Uul are mainly composed of quartz, kaolinite and illite, with a minor proportion of feldspars (Table 1 and Fig. 5). On the XRD pattern of the clay fractions, the asymmetry of the 10 Å and 5 Å reflection peaks indicate the presence of illite-smectite mixed layer phase (Fig. 6)

Sample BO24O and BOGD12 from Bitut location are mostly composed of quartz, illite and kaolinite (Table 1 and Fig. 5). The XRD pattern of the clay fraction of sample BO24O has very low intensity and display a broad peak between 12 Å to 20 Å indicating the presence of stacking disordered smectite (montmorillonite) (Fig. 6). The index of illite crystallinity (IC) (Kübler, 1964, 1967) measures changes in the full-width at half maximum intensity (FWHM) of the first basal reflection of dioctahedral illite-mica at 9.9 Å (Abad, 2007). The illite peak becomes broader as the crystallites get smaller and this causes the IC to be higher. The Illite Crystallinity (IC) has been determined for each pattern after decomposition of the reflections around 10 Å in order to exclude illite/smectite mixed layer reflections (Table 1). It can be seen in Table 1, that IC values measured on the clay fraction from the fault gouges are higher (peaks are broader) than that from the protolith from the same outcrop.

4.2. Microstructural characteristics (SEM)

The gouge samples display a heterogeneous microstructure that can be divided into two groups: cataclastic zone and clay gouge (represented as Backscattered Electron images in Figs. 7–9). Note that the boundary between the two zones can be progressive (Fig. 9).

Table 1
Mineralogical composition of the studied samples from XRD analyses on bulk powder and on the clay fractions.

		Bulk rock						Clay fraction			
		Quartz	Felsdpar	Mica	Kaolinite	Ankerite	Smectite and/or IS	Smectite	Illite	Kaolinite	IC
Noyon Uul											
BO17	Compacted host rock	***	***		**	**	*	**		***	
BO20B	Fragmented host rock	***	**	*	**	**	*		**	***	0.42
BO13C	Fault F1 black gouge	***	*	*	**	*	*	*	**	***	0.46
BO19	Fault F1 black gouge	***	**	*	***				**	***	0.54
BO20D	Fault F0 black gouge	***	*	*	**		*		**	***	0.64
BO20E	Fault F0 black gouge	***	*	*	**				***	***	0.6
Bitut											
BO24H	Host rock	***	_	***	**	**		*	**	***	0.29
BO24O, BO24N, BO25A	Thin black gouge	***		*	***		*	**	*	*	0.32
BOGD126, BO26F	Thick foliated gouge	***		**	**	*			**	***	0.37

***very abundant, **abundant, *present, IS: smectite/illite interstratified.

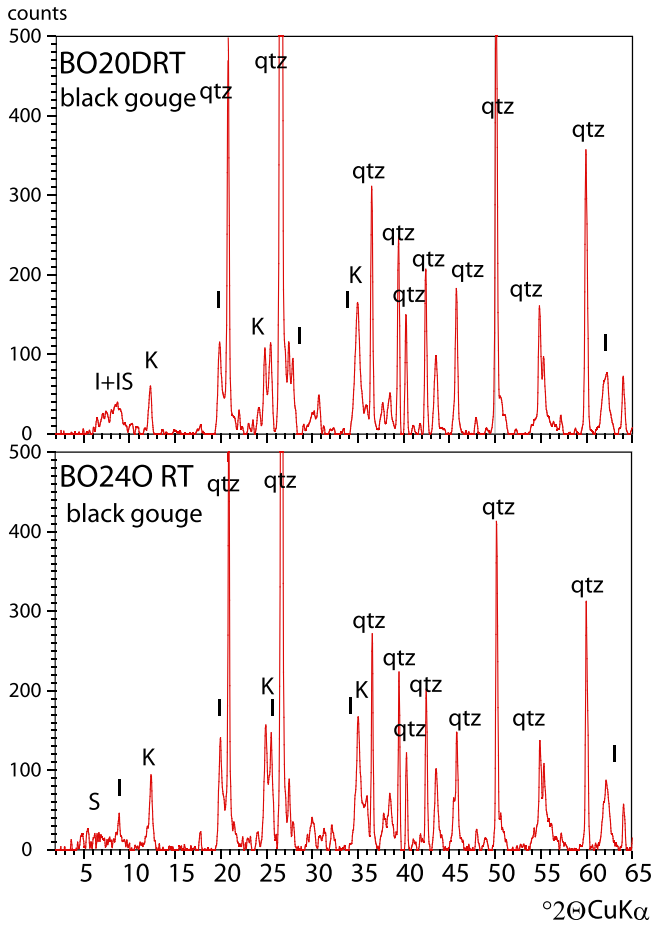

Fig. 5. X-ray diffraction patterns of bulk samples of black gouge from Noyon Uul (BO20DRT) and Bitut (BO24ORT). S: smectite, I: illite, K: kaolinite, Qtz : quartz, F: feldspar.

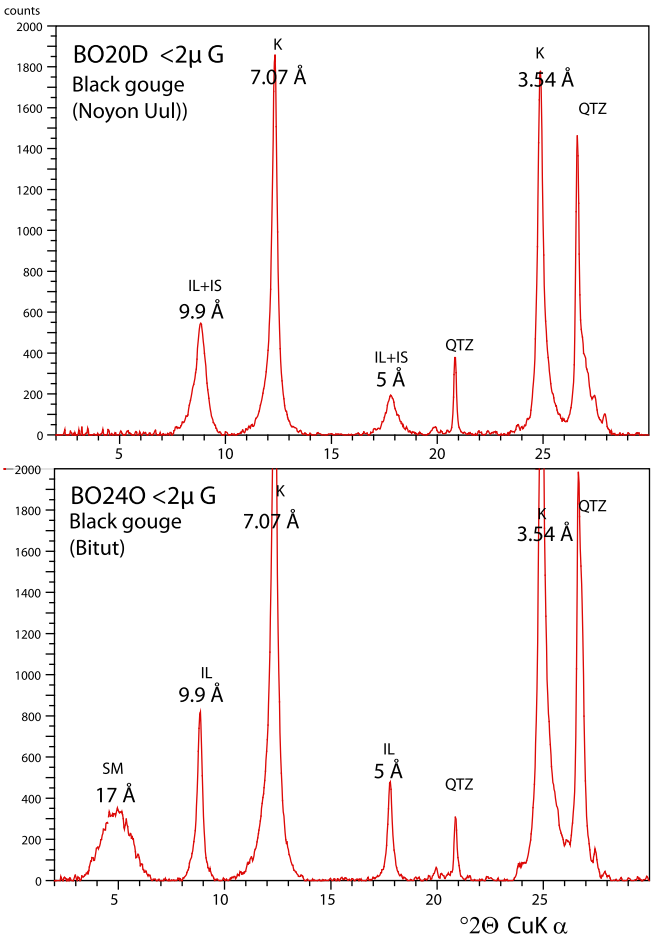

Fig. 6. X-ray diffraction patterns of oriented clay fraction of the gouge samples (after glycolation) from Noyon Uul (BO20D < 2µmG) and Bitut (BO24O < 2µmG) SM: smectite, IL: Illite, IS: Illite-smectite mixed layers, K : kaolinite, QTZ: quartz.

4.2.1. Cataclasite zone

The thick black gouge from Bitut has cataclastic microstructure with relict of the protolith mica schist and quartz grains in various sizes (Fig. 7A). Elongated micas (~100 µm) are commonly observed and preferentially oriented, which can be related to the relic texture of the ancient mica schist. Large quartz grains (>300 µm) are highly fractured with angular shape, suggesting a fragmentation process without displacements (Fig. 7B, C and E). The cataclasite zone is also characterized by the occurrence of authigenic kaolinite that fills the interstices between fragmented quartz grains. Small kaolinite grains (<5 µm) are mostly randomly oriented in the matrix (Fig. 7D, E and F). Small feldspar grains are sometimes observed in the kaolinite-rich area (Fig. 7B and D). They have irregular boundaries suggesting that they correspond to inherited relicts from partially dissolved feldspars (Fig. 7D). Locally, veins of iron oxides (ox) crosscut the cataclasites in different directions, suggesting that they formed later in the fault history (Fig. 8).

4.2.2. Clay gouges

The clay gouges are characterized by a homogeneous microstructure with less than 30% of grain fragments included within a matrix of very fine-grained material (10–20 µm) (Fig. 9). There are also two main types: foliated and isotropic gouges. The matrix of the foliated gouges displays some preferentially oriented clay minerals with sigmoidal geometry suggesting a shearing history (Fig. 9B). This type of microstructure is particularly well-expressed in samples BOGD12 and BO26 from Bitut (Fig. 9A). However, samples from Noyan Uul (e.g. BO20E) have an isotropic microstructure, with a dominant clay matrix that contained quartz grains less than 50 µm in size (Fig. 9C). The BE-SEM images of the gouge sample BO25 (Fig. 9B) shows an alternating texture varying from very fine-grained layers with homogeneous texture and foliated layers. The transition between these two textures is frequently progressive.

In the thick foliated gouge of Bitut, a kaolinite-rich zone can be easily identified (Fig. 9B, D and E), because of their lower electronic contrast compared to the illite/montmorillonite rich area. Elongated kaolinite aggregates align parallel to the shear surface, suggesting some degree of preferred orientation. The schistosity (SC) is recognized by the preferred orientation of small relict micas and clay minerals, which can be clearly observed in Fig. 9D and E. BE-SEM micrographs illustrate isotropic microstructure and foliated fabric of a thin Bitut gouge. In addition, high magnification SEM images (X4000) reveal that the clay-rich matrix contains a large amount of very fine-grained (<1 µm) and fragmented quartz crystals (Fig. 9F). Overall, the clay matrix clearly displays some degree of preferred orientation but the quantitative texture of clay minerals cannot be determined by this method.

4.3. TEM observations

Sample BO24O and BO20D were analyzed with the TEM to obtain high-resolution images for clay minerals microstructure in the fault gouges (Figs. 10 and 11). In both ion-milled and

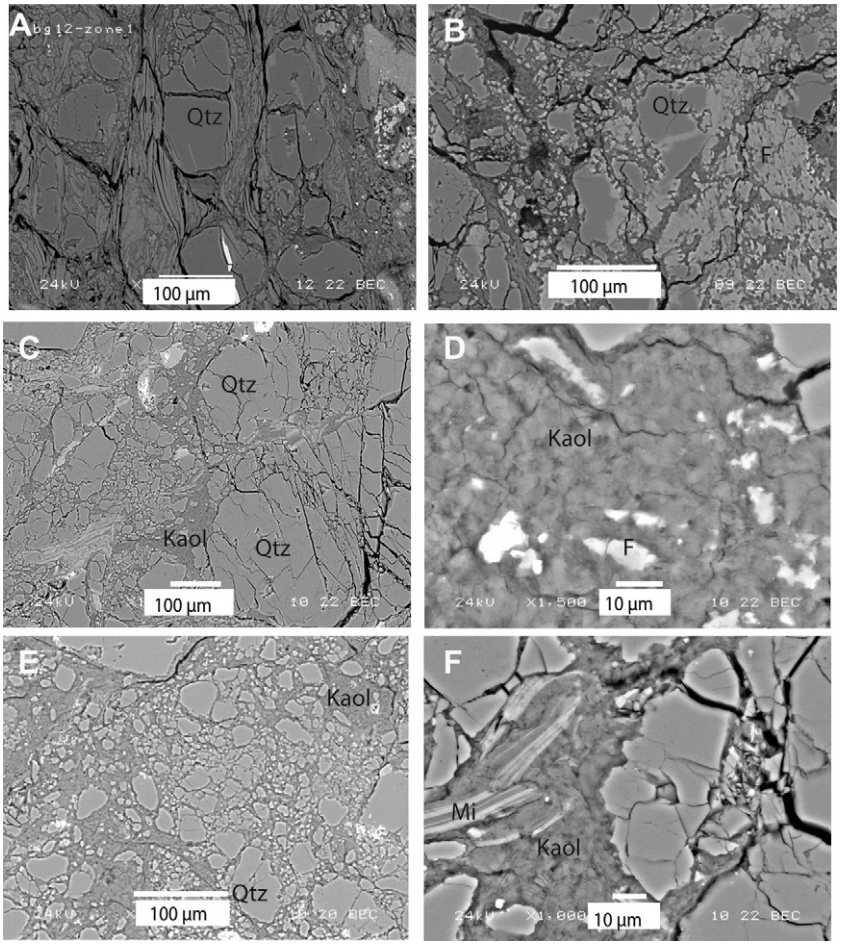

Fig. 7. SEM-BSE images of the cataclasite zone from the gouge samples. A. oriented mica and fragmented quartz in sample BOGD12 (Bitut). B. Highly altered feldspars in sample BOGD12 from Bitut C fractured quartz grains and kaolinite filling porosity (sample BO26). D. Authigenic kaolinite and small feldspar relics (sample BOGD12). E. Highly fragmented quartz grains (BO26). F. authigenic kaolinite and detrital Mica (BO26). Qtz: quartz, Mi: mica, F: feldspar, Kaol: kaolinite.

microtomed samples, small quartz grains of less than 0.5 µm are surrounded by very fine-grained and poorly crystallized clay particles, identified as CL in Fig. 10A and B. At least three different types of clays (mica Mi, kaolinite Kaol and montmorillonite and/or illite-smectite mixed layers (IS) are observed throughout the samples (Figs. 10 and 11). Micas of about 300 nm diameter are often found to be mixed with small clay particles. Clay minerals also tend to orient themselves parallel to quartz grain boundaries (Fig. 10D).

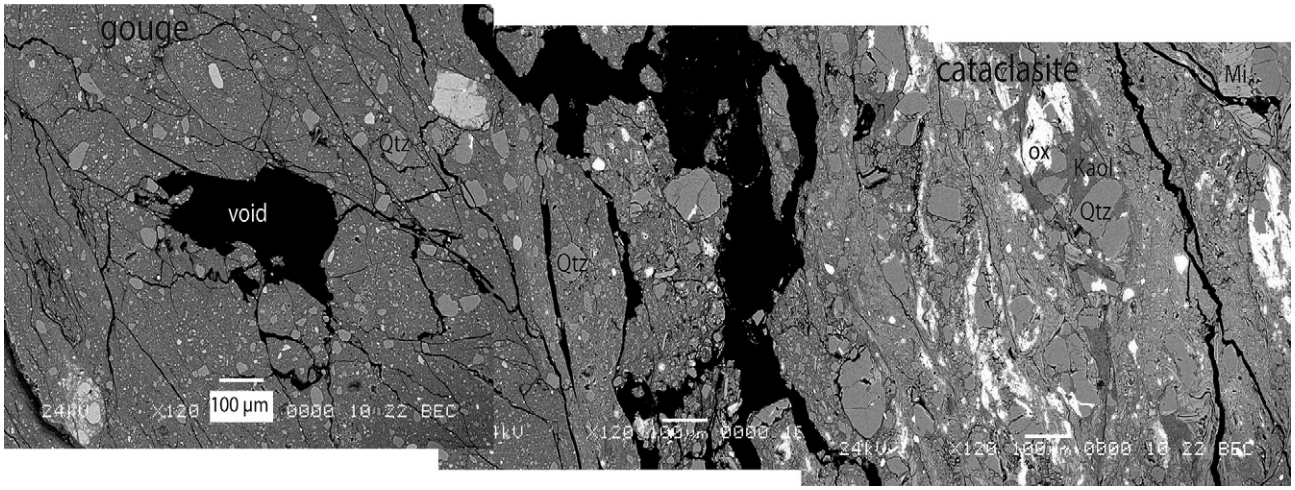

Fig. 8. SEM-BSE image at low magnification of the transition between cataclasite and gouge texture in sample BO25 (Bitut). The black area corresponds to holes (artifact related to the thin section preparation). Ox: Fe oxides, Kaol: kaolinite, Qtz: quartz.

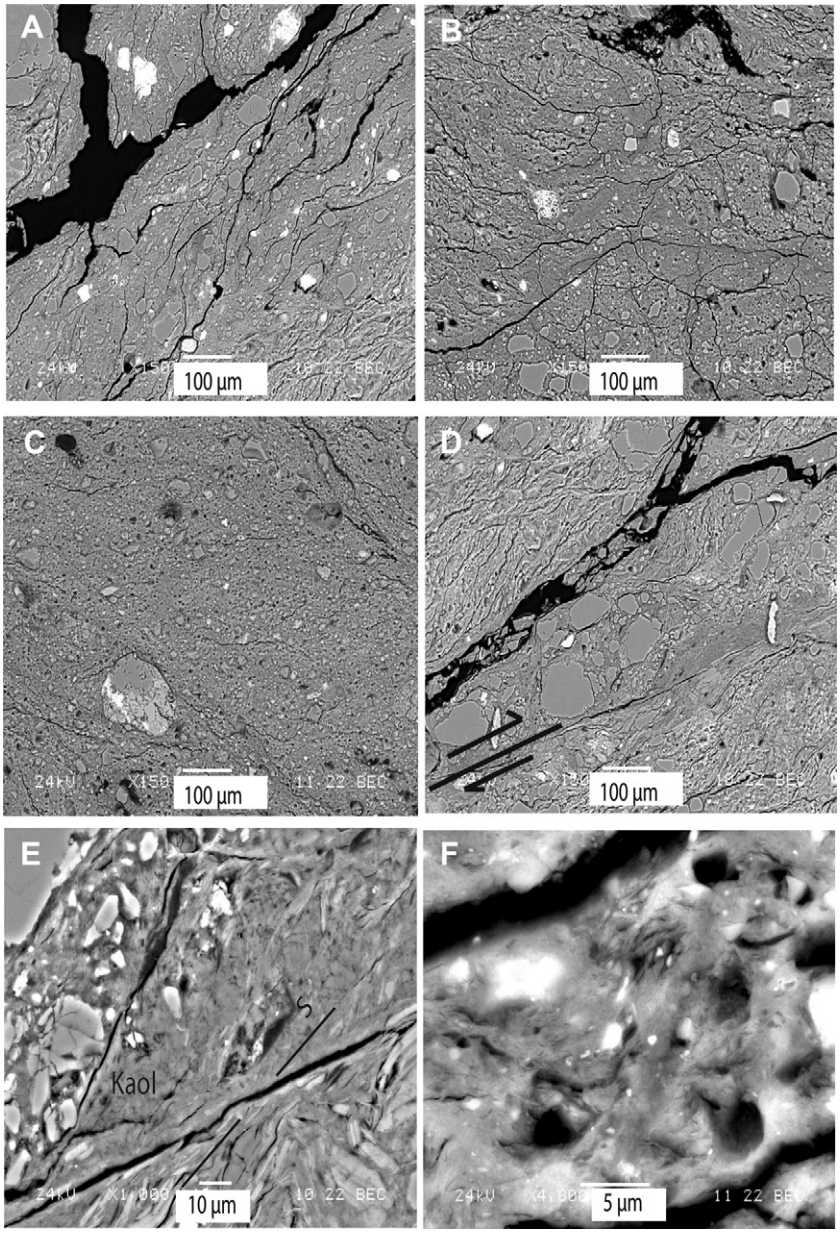

Fig. 9. Texture of the gouges at low magnification (A, B, C and D), and high magnification (E and F). A. Thick foliated gouge from Bitut (sample BO26), B. Thin gouge from Bitut with intermediate texture (sample BO25). C. Gouge from Noyon Uul with isotropic texture (sample BO20F). D and E show the textural arrangement of kaolinite along shear zone. F. Gouge of sample BO25 at high magnification.

Kaolinite is characterized by its strong sensitivity to electron beam damage. On the ion-milled samples, porosity can be observed at grain boundary interfaces (Fig. 10). This particular microtexture confirms that clay minerals have been affected by a fracturation and brecciation episode. Similar TEM microstructures have been observed in SAFOD core samples by Janssen et al. (2011). Fig. 11A shows the alignment of clay particles in sample BO20D, which help define the foliation in the sample. A high-resolution TEM image also reveals that these clay particles (~0.1 µm) are composed of regular stacking of 5–9 layers with 10 Å periodicity, suggesting the presence of illite (IL on Fig. 11B). Micas with a 2M polytype are also identified with a regular stacking of about 10–20 layers and ranging 0.5 to 1 micron µm in size (Fig. 11C). Irregular stacking of multiple layers with 10–13 Å periodicity are also observed in samples from the Bitut gouge (Fig. 11D). This characteristic indicates the presence of smectite or illite-smectite mixed layers (SM).

4.4. Texture measurements

All investigated samples (BO20E, BO24O and BO20D) are composed of over 5 mineral phases (Fig. 12 bottom). There are a large amount of smectite (montmorillonite), kaolinite and illite-mica (fragments are 5–70 µm in size). The (001) diffraction peaks of montmorillonite at ~14 Å are diffuse (Fig. 12), indicating small grain size and considerable stacking disorder. With the Rietveld method (Rietveld, 1969) it was possible to model turbostatically stacking disorder of this particular clay phase (Lutterotti et al., 2010). Other phases such as andesine and quartz are subordinate (5–10 wt %). Lattice parameters of the major phases were refined and correspond to those described in the literatures.

We also observed x-ray intensity changes with azimuth along some Debye rings, which indicate the preferred orientation of

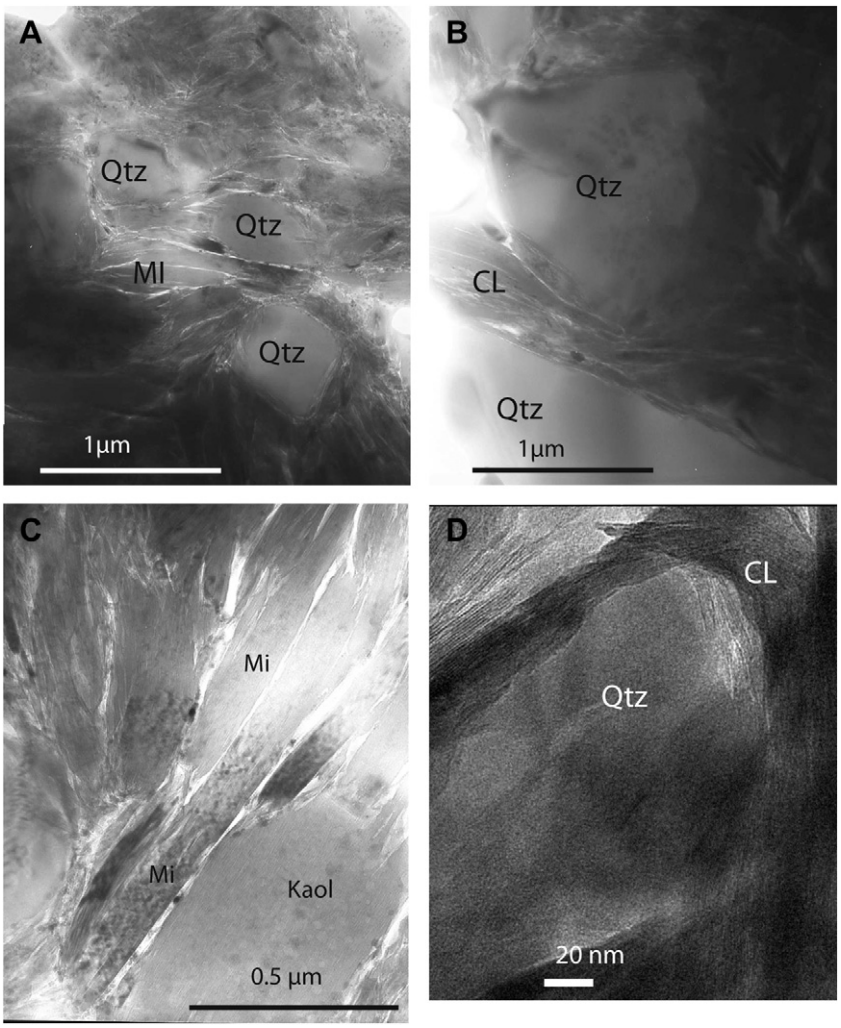

Fig. 10. TEM images of sample BO25 (ionmilled sample) showing the textural arrangement of the gouge matrix at a micrometric scale. A. Rounded quartz grains of 0.5 µm in diameter are surrounded by phyllosilicates. B. Detail of the clay-quartz contact. C. Detrital micas and kaolinite crystal with preferential orientation. Notice that porosity is visible between grain boundaries. D. Clay smearing of quartz fragment. CL: clay (undistinguished), Mi: Mica, Kaol: kaolinite, Qtz: quartz.

corresponding lattice planes *hkl*. This is best seen in a stack of diffraction spectra as function of azimuth corresponding to an "unrolled" diffraction image (Fig. 12A). Based on Rietveld analysis (Rietveld, 1969), the refined model diffraction spectra (top: Calc.) are compared with experimental spectra (bottom: Exp.) in Fig. 12A, which shows a close similarity, indicative of an excellent fit, both in intensities as well as position of diffraction peaks. Note intensity changes for clay minerals, but not for quartz. The quality of the fit is further quantified in Fig. 12B, which displays the average spectra for the 0° tilt image with dots for experimental data, and a thin solid line giving the calculated fit.

Pole figures are displayed for montmorillonite (Fig. 13A, D and G), illite-mica (Fig. 13B, E and H) and kaolinite (Fig.13C, F and I). In general, preferred orientation for phyllosilicate minerals are quite weak and asymmetric whereas orientation of quartz and andesine are close to random (pole figures are not shown). Kaolinite has a stronger texture than illite-mica in all samples. There is some variation between samples. Kaolinite in BO20D has the strongest texture with a (001) maximum perpendicular to the foliation of 2.6 multiples of a random distribution (m.r.d.). Orientation distributions of montmorillonite are quite weak in all samples, but most relevant in BO24O with 1.9 m.r.d. (Fig. 13D). In all samples a-axes spin randomly around the poles to (001).

5. Discussion

5.1. Origin of clay minerals

The mineralogical investigation of the Bitut and Noyan Uul samples suggests that the fault gouges and protoliths are composed of two clay types (1) the 2:1 type layers corresponding to smectite (montmorillonite), illite and illite-smectite mixed layers, and (2) the 1:1 type layers corresponding to kaolinite.

Montmorillonite and illite-smectite are present in various proportions in protolith and gouges. The BO17 sample from Noyan Uul, which is located in the damaged zone of the fault, has a significant amount of montmorillonite, inferring that this rock has undergone strong interaction with water (i.e. meteoritic or hydrothermal alteration). However, montmorillonite and illite-smectite are generally less abundant in the most deformed zone at Noyan Uul. At Bitut, the thin black gouge sample (BO24O) from Bitut samples also has a considerable amount of montmorillonite. This has been confirmed by TEM images, which show the occurrence of semi-ordered clay particles that could correspond to authigenic montmorillonite-like minerals. Smectite in the thin black gouge of Bitut could be inherited from the protolith or could be formed from fluids in the gouges.

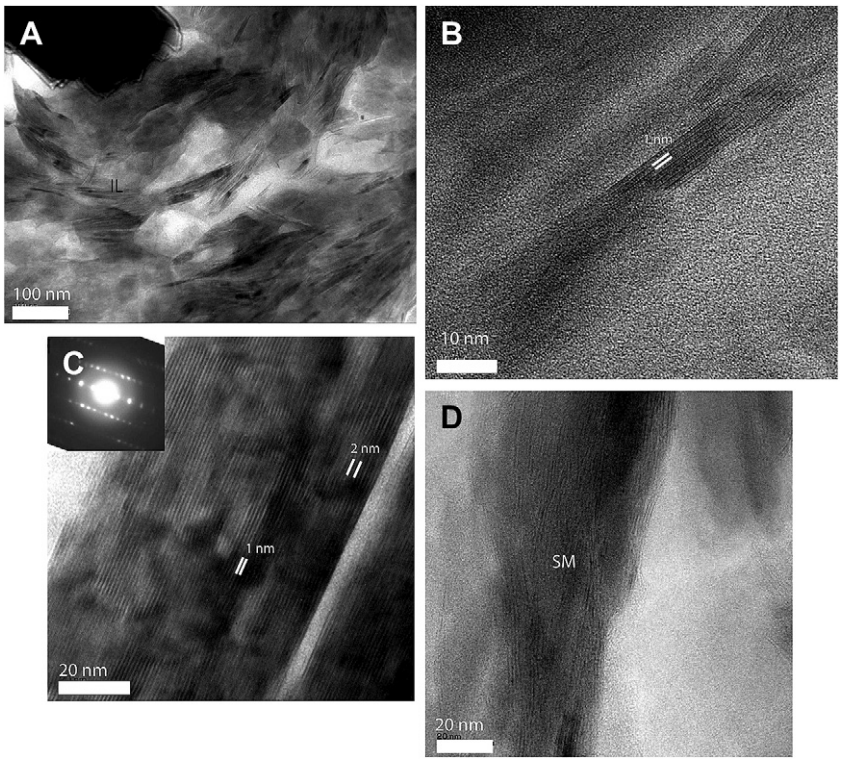

Fig. 11. TEM images of microtomed samples. A. Small crystallite of clay minerals (illite) in the clay matrix of sample BO20D from Noyon Uul. B. High resolution image of an illite crystallite (newly formed ?). C. Detrital mica with 2M polytype in sample BO20D. Electron diffraction pattern of the crystal is showed on the left side of the picture. D. Smectite or illite-smectite mixed layer in sample BO25 from Bitut.

Kaolinite is present in all samples and can be directly precipitated from fluids. It generally occurs as filling of the pores in cataclasites and as deformed lenses in thin black gouges. These observations imply that kaolinite has been formed between two deformation events, for example, as a result of fluid circulation in permeable structures created by the cataclastic deformation. The presence of ankerite in the protolith adjacent to the fault is another evidence, suggesting that the damaged zone of the fault was exposed to the circulation of meteoric or hydrothermal fluids. The presence of clay aggregates along the shearing planes in the cataclastic zone infers that they facilitate development of shear planes and the sliding mechanism of faults.

The origin of illite in the protolith and black gouges of the studied outcrops is more complex. In the gouges, it is formed as a result of fragmentation of muscovite particles that were initially present in protolith. The characterization of 2M polytype for some of the illite particles confirmed that the particles are inherited, i.e. their formation occurred at high temperature and pressure and can be related to the early metamorphism and deformation history. The diagenetic-metamorphic conditions can be investigated by measuring the crystalline domain size of illite. An increase of the IC was documented by Abad et al. (2003a,b) in phyllonite, located very close to a thrust plane, as a result of reducing of crystallite size and increase of lattice defect in illite during deformation. We observe a similar trend in our samples and it can thus be related to fault history. Particularly, in Bitut samples, the thin black gouge sample BO24O has higher IC (or poorer crystallinity; 0.32) than that of the host rock sample BO24H (0.29). This infers a strong reduction of particle size during deformation. The evidence of the 2M polytypes of some illite particles from the black gouges observed by TEM (Fig. 11) suggests that the major part of illite is inherited from fragmentation of metamorphic micas. However, in the Noyan Uul sample, TEM images show that small particles of illite are abundant (Fig. 13). Their morphology and their 1M stacking sequences as well as their texture suggest a possible synkinematic origin (Hower et al., 1963; Pevear, 1999).

5.2. Behavior of phyllosilicates

Three fault gouges (BO20E, BO24O and BO20D) which were analyzed for texture have similar mineralogical composition with dominating illite-mica (28.68–46.48 wt%). Overall, the fault gouge fabrics are weak and asymmetric, with maxima on (001) pole figures ranging from 1.27 m.r.d. in montmorillonite to 2.61 m.r.d. in kaolinite (Fig. 13). Minimum pole densities are from 0.42 m.r.d. to 0.78 m.r.d. indicating a large number of randomly oriented crystals. The texture strength of Bogd fault gouge is consistent with the previous synchrotron study of the San Andreas fault gouges (1.5–2.5 m.r.d.) (Wenk et al., 2010), as well as studies by X-ray texture goniometry for the Punchbowl fault from California (Van der Pluijm et al., 1994; Solum et al., 2003: 2–3.5 m.r.d.), the Death Valley area and West Salton detachments from California (Haines et al., 2009: 1.7–4.5 m.r.d.), the Moab fault from Utah (Solum et al., 2005: 1.8–5 m.r.d.), the Lewis thrust from Canada (Yan et al., 2001: 2–4 m.r.d.), the Caboneras fault from Spain (Solum and van der Pluijm, 2004: 2–7 m.r.d.), the Nojima fault from Japan (Shimamoto et al., 2001) and the Alpine fault from New Zealand (Warr and Cox, 2001).

A considerable amount of stacking disordered montmorillonite (12.43–21.68 wt%) is observed by a weak, broad and strongly asymmetric peak at 14 Å. This indicates interlayer water in the clay structure, suggesting a hydrothermal alteration history. The effect of stacking disorder is taken into account for texture analysis by introducing 10 layers along the stacking direction (Lutterotti et al., 2010). There is a noticeable texture variation between each clay phases, but kaolinite generally displays a stronger (001) texture

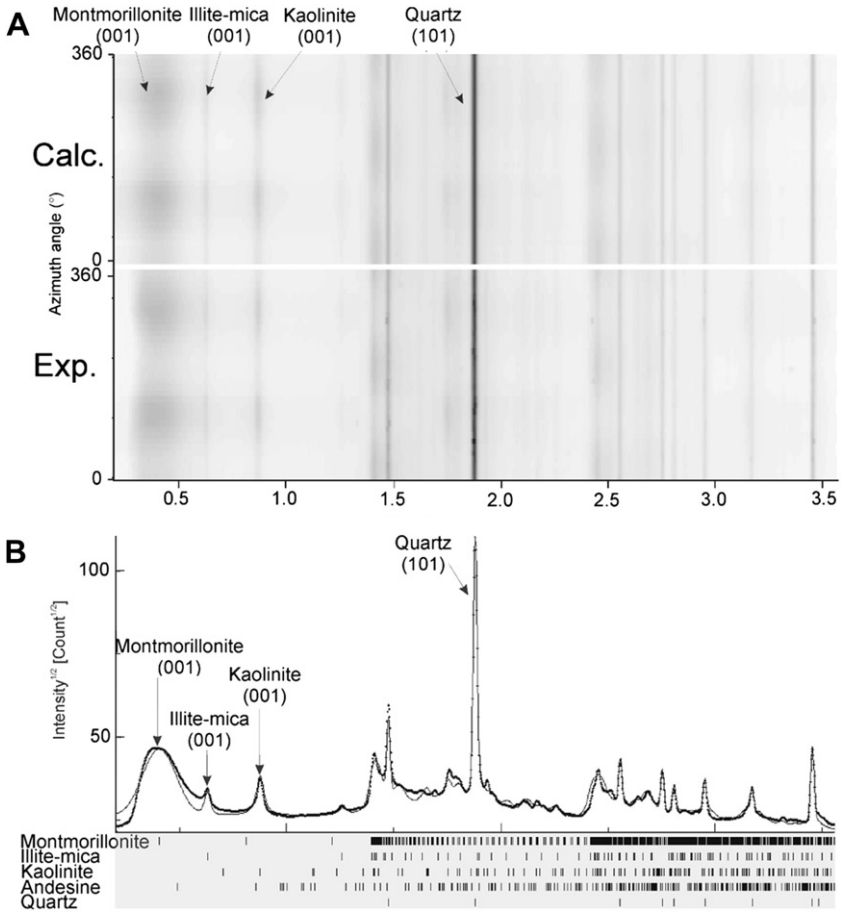

Fig. 12. A. Diffraction images showing variation of intensity along Debye rings. B. Map 2D plots of calculated (top) and experimental (bottom) diffraction spectra. C. Average diffraction spectra showing experimental data (dotted line) and calculated (solid line) models for BO20D sample.

(Wenk et al., 2010), as is the case in this Bogd fault gouge. The asymmetric pole figures of the constituent clays are referred to the orientation of sample slab. The SEM observations suggest that fabrics of clays are local and heterogeneous, and thus the foliation was difficult to ascertain. Moreover, texture of quartz and andesine are random. It has been shown that the presence of water-bearing minerals in gouge can affect the frictional resistance of the fault (Bird, 1984). Morrow et al. (2000) describes experiments with dry sheet structure minerals in presence of water and show that these minerals can decrease the frictional resistance of the gouge

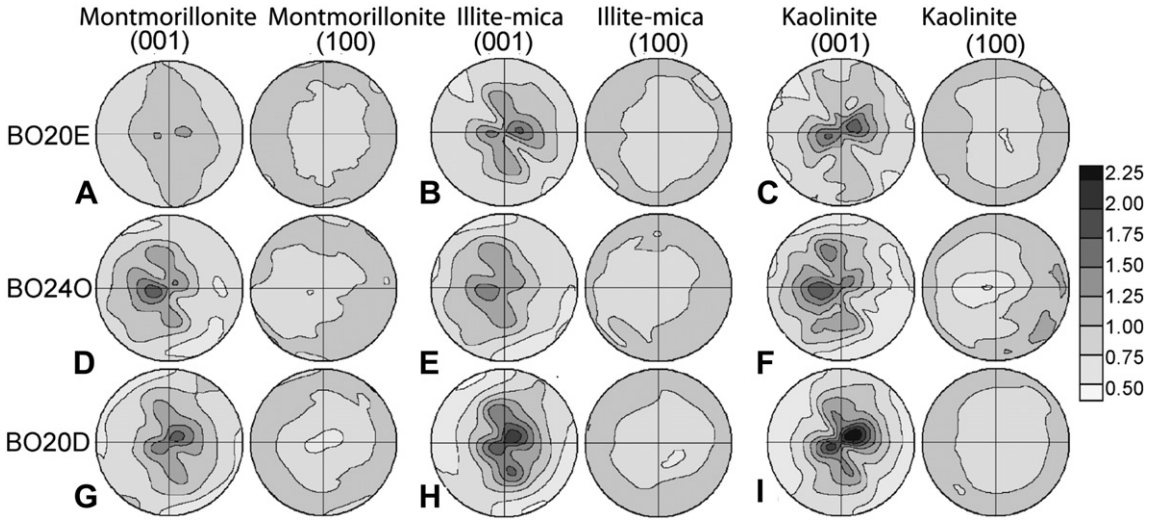

Fig. 13. (100) and (001) pole figures for montmorillonite, illite-mica, and kaolinite from the OD of BO20E (A, B, C), BO24O (D, E, F) and BO20D (G, H, I) samples. Contours in multiples of a random distribution (m.r.d.).

material. The temperature reached during frictional heating during a seismic event is able to create melting of the host rock (pseudotachylite) (Sibson, 1975) or to cause clay minerals dehydration (Brantut et al., 2008; Hirono et al., 2008). However, the product resulting from such dehydration is generally amorphous. Brantut et al. (2008) study the frictional behavior of kaolinite and suggest that dehydration and amorphization of kaolinite occurs at co-seismic slip of 1 m/s Hirono et al. (2008) investigate the kinetics of reaction of clay minerals during frictional heating and find that at temperatures below 200 °C, montmorillonite dehydration is possible in less than 10^5 s, whereas at temperatures higher than 800°, dehydroxylation of kaolinite and smectite can occur in a short time, but illitization of montmorillonite requires much longer time. In the Taiwan Chelungpu active fault, the decrease of kaolinite and smectite in the gouge is explained by the frictional heating during earthquake (Hirono et al., 2008). In this study, we conclude that fragmentation of constituent minerals is one of the deformation mechanisms in the Bogd and paleo-Bogd gouges. This brittle activity of the fault allows strong fragmentation of inherited phyllosilicates from the host rock. For example, 2M polytype micas were formed in the protolith during the ductile stage of deformation (shear zone). Kaolinite is present in all samples, suggesting that the studied gouges were not submitted to frictional heating conditions as in the experiments of Brantut et al. (2008). Our microstructure observations and texture measurements suggest that the Bogd and paleo-Bogd faults underwent polyphase deformation processes with high fragmentation (communication process) of grains during brittle activity and fault creeping episodes alternating with fluid circulation, which precipitated different clay components as a result.

5.3. The role of clay minerals on fault weakening

Holdsworth et al. (2011) investigate the microstructures of samples from the San Andreas fault drilled at 3 km depth and find a very similar texture to that described in the present study, with smectite derived from fluid related processes and fault weakening and chemical alteration processes. In the San Andreas fault, smectite forms interconnected networks of locally aligned phyllosilicates which can yield significantly lower friction coefficient. The amount of clay minerals in fault rocks can influence the frictional fault strength (Morrow et al., 2007; Tembe et al., 2006). Solum et al. (2010) provide evidence for authigenesis of clays in the Moab fault and they show that this process can lead to a significant increase of the clays content on fault and consequently induce a fault weakening. The relationship between frictional strength and clay mineralogy in natural fault gouge has been investigated by Numelin et al. (2004). The friction coefficient is measured at normal stress from 5 to 150 MPa. They find a coefficient of 0.2–0.4 for samples containing more than 50 total clay content, whereas for most samples with lower clay content the friction coefficient is about 0.6–0.7, consistent with Byerlee's law. Montmorillonite, which can take on large amounts of interlayer water, has a coefficient of friction, μ of only 0.2 at room temperature under moderate pressure conditions. Morrow et al. (2000) demonstrate that the friction coefficient decreases more than 60% for montmorillonite in the presence of adsorbed water.

Illitization of montmorillonite is suspected in the gouge sample from Noyan Uul. The preferred orientation of the illite particles suggests that they formed during post seismic creeping. Montmorillonite-illite transition is generally observed in pelite which underwent progressive burial (Ahn and Peacor, 1989). This transition is usually related to temperature increase and chemical transfer through fluids (Buatier et al., 1992). Vrolijik and van der Pluijm, (1999) suggest that kinetic energy supplied by fault activity could allow montmorillonite transformation to illite in fault gouges. Dellisanti et al. (2008) describe illitization of smectite facilitated by the preferential orientation of phyllosilicates along planar discontinuities, which circulates the fluids and permits the dissolution of smectite and recrystallization of illite. Saffer and Marone (2003) compared the frictional properties of smectite and illite rich gouges. They found a lower friction coefficient for montmorillonite but they did not observed any transition from velocity strengthening to velocity weakening behavior during smectite to illite transition. Based on the results of Lockner et al. (2006), Solum et al. (2010) speculate that the transition from montmorillonite to illite would cause a change from stick-slip to creeping fault behavior.

6. Conclusions

This study demonstrates that the protoliths and the fault gouges of the Bogd and paleo-Bogd faults were highly altered by fluids. The fluid-rock interactions allow the formation of clay minerals and the alteration of feldspars, which precipitated kaolinite and montmorillonite. This alteration occurs between two deformation episodes and affects the protolith and the fault zone. Micas are present in all samples and can be observed as fragmented inherited 2M muscovite grains in the protoliths. In some highly deformed samples from Noyan Uul, the presence of newly formed synkinematic illite is suspected. The decrease of montmorillonite fractions in highly deformed samples from Noyan Uul implies dehydration process during deformation leading to illite precipitation. Microstructures are quite heterogeneous with foliated microscopic zones alternating with isotropic clay-rich areas. The clay textures have (001) maxima ranging from 1.27 m.r.d. to 2.61 m.r.d. Kaolinite has the strongest texture while montmorillonite has the weakest textural strength in all samples. Co-existing quartz and andesine have random textures. These observations suggest that the studied fault registered brittle and ductile deformation although aseismic creep along the Bogd and paleo-Bogd faults systems was not detected with the classical morphotectonic methods. The clays minerals, which are the major component of the gouge, are mostly related to the circulation of fluid. Their presence may favor the slip weakening behavior of the fault.

Acknowledgments

The authors thank Remi Chassagnon and Nicolas Rouge for their technical assistance on the TEM (ULB) and SEM (UFC) analyses. HRW acknowledges support from NSF (EAR-0836402) and DOE (DE-FG02-05ER15637). We are appreciative for access to beamline 11-ID-C at the Advanced Photon Source and assistance from Yang Ren for synchrotron diffraction experiments. We are grateful for the constructive reviews provided by John Solum and an anonymous reviewer.

References

Abad, I., Gutierrez-Alonso, G., Nieto, F., Gertner, I., Becker, A., Cabero, A., 2003a. The structure and the phyllosilicates (chemistry, crystallinity and texture) of Talas Ala-Tau (Tien Shan, Kyrgyz Republic): comparison with more recent subduction complexes. Tectonophysics 365 Issue: 1–4 Sp. Iss. 103–127.

Abad, I., Nieto, F., Gutierrez-Alonso, G., Do Campo, M., Lopez-Munguira, A., Velilla, N., 2003b. Prograde and retrograde diagenetic and metamorphic evolution in inetapelitic rocks of Sierra Espuna (Spain). Clay Minerals 38, 59–69.

Abad, I., 2007. Physical meaning and applications of the illite Kubler index: measuring reaction progress in low-grade metamorphism. In: Jiménez-Millán, F.N.a.J. (Ed.), Diagenesis and Low-Temperature Metamorphism. Theory, Methods and Regional Aspects. Seminarios de la Sociedad Española de Mineralogía, Jaén, pp. 53–64.

Ahn, J.H., Peacor, D.R., 1989. Illite/smectite from the Gulf Coast shales: a reappraisal of transmission electron microscope images. Clays and Clay Minerals 37, 542–546.
Buatier, M.D., Peacor, D., O'Neil, J.R., 1992. Smectite-illite transition in Barbados accretionary wedge sediments: TEM and AEM evidence for dissolution/crystallization at low temperature. Clays and Clay Minerals 40, 65–80.
Bird, P., 1984. Hydration-phase diagrams and friction of montmorillonite under laboratory and geologic conditions, with implications for shale compaction, slope, stability and strength of fault gouge. Tectonophysics 107, 235–260.
Bish, D.L., 1993. Rietveld refinement of kaolinite structure at 1.5 K. Clays and Clay Minerals 41, 738–744.
Baljinnyam, I., Bayasgalan, A., Borisov, B.A., Cisternas, A., Dem'yanovich, M.G., Ganbaatar, L., Kochetkov, V.M., Kurushin, R.A., Molnar, P., Philip, H., Vashchilov, Yu. Ya., 1993. Ruptures of major earthquakes and active deformation in Mongolia and its surroundings. Geological Society of America Memoir 181.
Brantut, N., Schubnel, A., Rouzaud, J.N., Brunet, F., Shimamoto, T., 2008. High-velocity frictional properties of a clay-bearing fault gouge and implications for earthquake mechanics. Journal of Geophysical Research –Solid Earth 113, B10.
Day-Stirrat, R.J., Aplin, A.C., Srodon, J., van der Pluijm, B.A., 2008. Diagenetic reorientation of phyllosilicate minerals in paleogene mudstones of the Podhale Basin, southern Poland. Clays and Clay Min. 56, 100–111.
Dellisanti, F., Pini, G.A., Tateo, F., Baudin, F., 2008. The role of tectonic shear strain on the illitization mechanism of mixed-layers illite-smectite. A case study from a fault zone in the Northern Apennines, Italy. International Journal of Earth Sciences 97, 601–616.
Elsass, F., Beaumont, A., Pernes, M., Jaunet, A.M., Tessier, D., 1988. Changes in layer organization of Na and Ca exchanged smectite during solvent exchange for embedment in resin. The Canadian Mineralogist 36, 1325–1333.
Florensov, N.A., Solonenko, V.P., 1965. The Gobi-Altay Earthquake. U.S. Dep. of Commer, Washington, D. C.
Gualtieri, A.F., 2000. Accuracy of XRPD QPA using the combined rietveld-RIR method. Journal of Applied Crystallography 33, 267–278.
Haines, S.H., van der Pluijm, B.A., Ikari, M., Saffer, D., Marone, C., 2009. Clay fabric intensity in natural and artificial fault gouge: implications for brittle fault zone processes and sedimentary basin clay fabric evolution. Journal of Geophysical Research 114, B05406.
Hirono, T., Fujimoto, K., Yokoyama, T., Hamada, Y., Tanikawa, W., Tadai, O., Mishima, T., Tanimizu, M., Lin, W., Soh, W., Song, S.R., 2008. Clay mineral reactions caused by frictional heating during an earthquake: an example from the Taiwan Chelungpu fault. Geophysical Research Letters 35, L16303. doi:10.1029/2008GL034476.
Hofmann, U., Endell, K., Wilm, D., 1933. Kristallstuktur and Qeullung von Montmorilonit. Zeitschrift für Kristallographie 86, 340–348.
Holdsworth, R.E., van Diggelen, EW.E., Spiers, C.J.J., de Bresser, J.H.P., Walker, R.J., Bowen, L., 2011. Fault rocks from the SAFOD core samples: implications for weakening at shallow depths along the San Andreas fault, California. Journal of Structural Geology 33, 132–144.
Hower, J., Hurley, P.M., Pinson, W.H., Fairbairn, H.W., 1963. The dependence of K-Ar age on the mineralogy of various particle size ranges in a shale. Geochimica et Cosmochimica Acta 27, 405–410.
Janssen, C., Wirth, R., Rybacki, E., Naumann, R., Kemnitz, H., Wenk, H.R., Dresen, G., 2010. Amorphous material in SAFOD core samples (San Andreas Fault): evidence for crush-origin pseudotachylytes? Geophysical Research Letters 37, L01303.
Janssen, C., Wirth, R., Reiniiicke, A., Rybacki, E., Naumann, R., Wenk, H.R., Dresen, G., 2011. Nanoscale porosity in SAFOD core samples (San Andreas Fault). Earth and Planetary Science Letters 301, 179–189.
Jolivet, M., Ritz, J.-F., Vassallo, R., Larroque, C., Braucher, R., Todbileg, M., Chauvet, A., Sue, C., Arnaud, N., De Vicente, R., Arzhannikova, A., Arzhannikov, S., 2007. The Mongolian summits: an uplifted, flat, old but still preserved erosion surface. Geology 35 (10), 871–874. doi:10.1130/G23758A.1.
Kanitpanyacharoen, W., Frans, K., Lehr, B.C., Wenk, H.R. in press. Texture and anistropy analysis of Qusaiba shales, Geophysical Prospecting.
Kurushin, R.A., Bayasgalan, A., lziybat, M.O., Enkhtuvshin, B., Molnar, P., Bayarsayhan, C., Hudnut, K.W., Lin, J., 1997. The surface rupture of the 1957 Gobi-Altay, Mongolia, earthquake. Special Paper - Geological Society of America 320.
KKüblerbler, B., 1964. Les argiles, indicateurs de métamorphisme. Revue Institut France Pétrol 19, 1093–1112.
KKüblerbler, B., 1967. La cristallinité de l'illite et les zones tout à fait supérieures du métamorphisme, 1966 métamorphisme, paper presented at Etages Tectoniques, Colloque de Neuchâtel 1966, Univ. Neuchâtel, á la Baconnière, Suisse.
Kübler, B., 1987. Cristallinité de l'illite, méthodes normalisées de préparations, méthodes normalisées de mesures. Institut de Géologie de Neuchâtel Série ADX, Cahier.
Lutterotti, L., Voltoni, M., Wenk, H.R., Bandyopadhyay, K., Vanorio, T., 2010. Texture analysis of a turbostratically disordered Ca-montmorillonite. American Mineralogist 95, 98–103.
Lutterrotti, L., Matties, S., Wenk, H.R., Schultz, A.J., Richardson, J.W., 1997. Combined texture and structure analysis of deformed limestone from time-of-flight neutron diffraction spectra. Journal of Applied Physics 81, 594–600.
Lockner, D., Solum, J.G., Davatzes, N., 2006. The effect of brine composition and concentration on strength of expandable clays. Eos Transactions AGU 87 (52) Fall meeting Suppl., Abstract T31F-03.
Mair, K., Abe, S., 2008. 3D numerical simulations of fault gouge evolution during shear: grain size reduction and strain localization. Earth and Planetary Science Letters 274 (1–2), 72–81.
Matthies, S., Vinel, G.W., 1982. On the reproduction of the orientation distribution function of textured samples from reduced pole figures using the concept of conditional ghost correction. Physica Status Solidi B 122, K111–K114.
Mizoguchi, K., Hirose, T., Shimamoto, T., Fukuyama, E., 2009. High-velocity frictional behavior and microstructure evolution of fault gouge obtained from Nojima fault, southwest Japan. Tectonophysics 471 (3–4), 285–296.
Morrow, C.A., Moore, D.E., Lockner, D.A., 2000. The effect of mineral bond strength and adsorbed water on fault gouge frictional strength. Geophysical Research Letters 27 (6), 815–818.
Morrow, C., Solum, J.G., Tembe, S., Lockner, D., Wong, T., 2007. Using drill cuttings separates to estimate the strength of narrow shear zones at SAFOD. Geophysical Research Letters 34, L11301. doi:10.1029/2007GL029665.
Numelin, T., Marone, C., Kirby, E., 2004. Frictional properties of natural fault gouge from a low-angle normal fault, Panamint Valley, California. Tectonics 26, 1–14.
Pevear, D.R., 1999. Illite and hydrocarbon exploration. Proceedings of the National Academy of Sciences of the United States of America 96, 3440–3446.
Popa, N.C., 1998. The (hkl) dependence of diffraction-line broadening cuased by strain and size for all Laue groups in Rietveld refinement. Journal of Applied Crystallography 31, 176–180.
Rice, J.R., 1992. Fault stress states, pore pressure distributions, and the weakness of San Andreas Fault. In: Evans, B., Wong, T.-F. (Eds.), Fault Mechanics and Transport Properties of Rocks: a Festschrift in Honor of W.F. Brace. Academic, San Diego, California, pp. 475–503.
Rietveld, H.M., 1969. A profile refinement method for nuclear and magnetic structures. Journal of Applied Crystallography 2, 65–71.
Ritz, J.-F., Brown, E.T., Bourlès, D.L., Philip, H., Schlupp, A., Raisbeck, G.M., Yiou, F., Enkhtuvshin, B., 1995. Slip rates along active faults estimated with cosmic-ray-exposure dates: application to the Bogd fault, Gobi-Altaï, Mongolia. Geology 23, 1019–1022.
Ritz, J.-F., Vassallo, R., Braucher, R., Brown, E.T., Carretier, S., Bourlès, D.L., 2006. Using in Situ-produced 10Be to Quantify active tectonics in the Gurvan Bogd mountain range (Gobi-Altay, Mongolia). In: Siame, L., Bourlès, D.L., Brown, E.T. (Eds.), Geological Soc.. of America Special Paper 415 "In Situ-produced Cosmogenic Nuclides and Quantification of Geological Processes", pp. 87–110.
Rutter, E.H., Maddock, R.H., Hall, S.H., White, S.H., 1986. Comparative microstructures of natural and experimentally produced clay-bearing fauly gouge. Pure and Applied Geophysics 124, 3–30.
Saffer, D.M., Marone, C., 2003. Comparison of smectite- and illite-rich gouge frictional properties: application to the updip limit of the seismogenic zone along subduction megathrusts. Earth and Planetary Science Letters 215, 219–235.
Schleicher, A.M., Warr, L.N., van der Pluijm, B.A., 2009. On the origin of mixed-layered clay minerals from the San Andreas Fault at 2.5-3 km vertical depth (SAFOD drillhole at Parkfield, California. Contributions to Mineralogy and Petrology. 157, 173–187.
Schulz, S.E., Evans, J.P., 1998. Spatial variability in microscopic deformation and composition of the Punchbowl fault, southern California: implications for mechanisms, fluid-rock interaction, and fault morphology. Tectonophysics 295, 223–244.
Shimamoto, T., Takemira, K., Fujimoto, K., Tanaka, H., Wibberley, C.A.J., 2001. Nojima Fault Zone probing by core analyses. The Island Arc, 357–359.
Sibson, R.H., 1975. Generation of pseudotachylite by ancient seismic faulting. Geophysical Journal of the Royal Astronomical Society 43, 775–794.
Solum, J.G., van der Pluijm, B.A., Peacor, D.R., Warr, L.N., 2003. Influence of phyllosilicate mineral assemblages, fabrics, and fluids on the behavior of the Punchbowl fault, southern California. Journal of Geophysical Research 108 (B5), 5–12.
Solum, J.G., van der Pluijm, B.A., 2004. Phyllosilicate mineral assemblages of the SAFOD Pilot hole and comparisons with an exhumed segment of the San Andreas Fault system. Geophysical Research Letter 31. doi:10.1029/2004GL019909.
Solum, J.G., van der Pluijm, B.A., Peacor, D.R., 2005. Neocrystallization, fabrics and age of clay minerals from an exposure of the Moab Fault, Utah. Journal of Structural Geology. 27, 1563–1576.
Solum, J.G., Davatzes, N., Lockner, D.A., 2010. Fault-related clay authigenesis along Moab fault: implications for calculations of fault rock composition and mechanical and hydrologic fault zone properties. Journal of Structural Geology 32, 1899–1911.
Tembe, S., Lockner, D.A., Solum, J.G., Morrow, C., Wong, T.-f., Moore, D.E., 2006. Frictional strength of cuttings and core from SAFOD drillhole phases 1 and 2. Geophysical Research Letters 33, L23307. doi:10.1029/2006GL027626.
Tessier, D., 1984. Hydratation, gonflement et structuration des matériaux argileux au cours de la dessication et de la réhumectation. Ph. D. thesis, Université de Paris & INRA Versailles, France.
Ufer, G., Roth, G., Kleeberg, R., Stanjek, H., Dohrmann, R., Bergmann, J., 2004. Description of X-ray powder pattern of turbostratically disordered layer structures with a rietvled compatible approach. Zeitschrift für Kristallographie 219, 519–527.
Van der Pluijm, B.A., Ho, N.C., Peacor, D.R., 1994. High resolution X-ray texture goniometry. Journal of Structural Geology 16, 1029–1032.
Voltolini, M., Wenk, H.R., Mondol, N.H., Bjolykke, K., Jahren, J., 2009. Anisotropy of experimentally compressed kaolinite-illite-quartz mixtures. Geophysics 74, 13–23.

Vassallo, R., Jolivet, M., Ritz, J.-F., Braucher, R., Larroque, C., Sue, C., Todbileg, M., Javkhlanbold, D., 2007a. Uplift age and rates of the Gurvan Bogd system (Gobi-Altay) by apatite fission track analysis. Earth and Planetary Science Letters 259, 3–4. doi:10.1016/j.epsl.2007.04.047. 333–346.

Vassallo, R., Ritz, J.-F., Braucher, R., Jolivet, M., Chauvet, A., Larroque, C., Carretier, S., Bourlès, D., Sue, C., Todbileg, M., Arzhannikova, N., Arzhannikov, S., 2007b. Transpressional tectonics and stream terraces of the Gobi-Altay, Mongolia. Tectonics 26, TC5013. doi:10.1029/2006TC002081.

Vrolijk, P., van der Pluijm, B.A., 1999. Clay gouge. Journal of Structural Geology 21, 1039–1048.

Warr, L.N., Cox, S., 2001. Clay mineral transformation and weakening mechanisms along the Alpine Fault, New Zealand. In: Holdsworth, R.E., Strachan, R.A., Magloughlin, J.F., Knipe, R.J. (Eds.), The Nature and Tectonic Significance of Fault Weakening. Geological Society, London, Special Publication, vol. 186, pp. 85–1001.

Wenk, H.-R., Matthies, S., Donovan, J., Chateigner, D., 1998. BEARTEX, a Windows-based program system for quantitative texture analysis. Journal of Applied Crystallography 31, 262–269.

Wenk, H.-R., Voltolini, M., Mazurek, M., Van Loon, L.R., Vinsot, A., 2008. Preferred orientations and anisotropy in shales: Callovo-Oxfordian shale (France) and Opalinus clay (Switzerland). Clays and Clay Minerals 56, 285–306.

Wenk, H.R., Kanitpanyacharoen, W., Voltolini, M., 2010. Preferred orientation of phyllosilicates: comparison of fault gouge, shale and schist. Journal of Structural Geology 32, 478–489.

Yan, Y., van der Pluijm, B.A., Peacor, D.R., 2001. Deformation microfabrics of clay gouge, Lewis Thrust, Canada: a case for fault weakening from clay transformation. In: Holdsworth, R.E., Strachan, R.A., Magloughlin, J.F., Knipe, R.J. (Eds.), The Nature and Tectonic Significance of Fault Zone Weakening. Special Publication Geological Society, London, vol. 186, pp. 103–112.